

Waves in Random and Complex Media


ISSN: (Print) (Online) Journal homepage: <https://www.tandfonline.com/loi/twrm20>

Simulation of forced convective power law fluid by using Darcy–Brinkman–Forchheimer flow model field


Farhan Ahmed, Rashid Mehmood & Ali J. Chamkha


To cite this article: Farhan Ahmed, Rashid Mehmood & Ali J. Chamkha (2022): Simulation of forced convective power law fluid by using Darcy–Brinkman–Forchheimer flow model field, Waves in Random and Complex Media, DOI: [10.1080/17455030.2022.2125596](https://doi.org/10.1080/17455030.2022.2125596)

To link to this article: <https://doi.org/10.1080/17455030.2022.2125596>

 Published online: 26 Sep 2022.

 Submit your article to this journal [↗](#)

 Article views: 26

 View related articles [↗](#)

 View Crossmark data [↗](#)



Simulation of forced convective power law fluid by using Darcy–Brinkman–Forchheimer flow model field

Farhan Ahmed^{a,b}, Rashid Mehmood^c and Ali J. Chamkha^d

^aDepartment of Mathematics, Government Degree College Sherwan Abbottabad, Abbottabad, Pakistan;

^bArchives and Libraries Department, Government of Khyberpakhtun Khwa Higher Education, Peshawar, Pakistan; ^cDepartment of Mathematics, Faculty of Natural Sciences, HITEC University, Taxila Cantt, Pakistan;

^dFaculty of Engineering, Kuwait College of Science and Technology, Doha District, Kuwait

ABSTRACT

This study investigates the fully developed heat transfer of steady, incompressible and laminar flow of power law fluid saturated porous medium through the rectangular duct by utilizing Darcy–Brinkman–Forchheimer flow model field. Hydrodynamic flow of power law-based fluid within a rectangular duct with porosity has not been reported in the literature. The consideration of Darcy–Brinkman–Forchheimer flow model makes it very much novel in its own right. The main objective of the present study is to explore the modified Darcy parameter on flow and heat transfer characteristics. Numerical results are obtained for different values of Darcy parameter, Da , inertia coefficient, Fr and power law model, n . We note the significant impact of inertial force on flow and heat transfer in the case of dilatant fluid; however, inertial force term can be ignored in the case of pseudo-plastic fluid due to its lower effect. Furthermore, with the decrease in aspect ratio, the effect of the inertial force can be reduced. It is also noted that, axial velocity significantly enhances with Darcy parameter Da . This behavior of the axial velocity is found to be similar for higher inertia coefficient Fr as well.

ARTICLE HISTORY

Received 17 November 2021
Accepted 6 September 2022

KEYWORDS

Rectangular duct; Darcy number; inertial force; friction factor; heat transfer rate

Introduction

Flow through porous media gets significant status due to their wide range of applications in engineering, technical and geophysics fields including the water movement in geothermal reservoirs, underground spreading of chemical waste, grain storage, drying, fuel cells and in the finding of petroleum reservoirs etc. Darcy flow model is applicable on almost all of the small pores media naturally. In the case of hand-made large pores media, the Brinkman model portends the hydraulics as discussed by [1].

Hooman et al. [2] studied the thermally developing flow by implying the Brinkman flow model for the determination of velocity field. Chen and Tso [3] discussed the thermally developing convection flow in the presence of porous media. Ouyang et al. [4] analyzed analytically thermally developing flow in porous media by using local thermal non-equilibrium condition.

CONTACT Farhan Ahmed  fahmed_math@yahoo.com

Naturally, most of the fluids exist in non-Newtonian and play important role in geophysics application. Therefore, scientists play a very important role in this case by studying the characteristics of power law fluid under different assumptions and geometries [5–12].

Kumar et al. [13] numerically analyzed the forced convective power law fluid in the range of power law model, 0.2 – 1.8 by using the Ansys fluent. They observed that Drag coefficient increases by increasing the power law model. Lin et al. [14] studied the laminar flow of non-Newtonian power law fluid over a flat plat with a new nonlinear diffusion model. Ahmed [15] studied the impact of uniform transverse magnetic field on the forced convective flow of power law fluid through the rectangular duct. They observed that the damping effect due to magnetic field is more effective in the case of dilatant fluid as compared to pseudo-plastic fluid. Furthermore, velocity decreases by increasing the value of the aspect ratio. Chen and Tso [16] numerically studied the impact of viscous dissipation on the forced convective power law fluid saturated porous medium. Elgazery [17] studied the unsteady free convection power law fluid by applying the Darcy–Brinkman–Forchheimer model to describe the flow field with the help of implicit-Chebyshev collocation spectral method. Kovetska et al. [18] considered the Darcy–Brinkman–Forchheimer model for film boiling in porous media and concluded that heat transfer in a porous medium at film boiling was less intensive compared to non-porous medium.

In most of the studies in the literature, scientists ignore the effect of inertial force due to lowered change in friction factor and heat transfer rate. In the case of non-Newtonian fluid, the inertial force effect on friction factor and heat transfer rate becomes pronounced. Main purpose of this study is to carry out the Darcy–Brinkman Forchheimer model on the flow field and heat transfer analysis of power law fluid saturated porous medium through the rectangular duct. The results are computed for different values of aspect ratio, Darcy parameter and inertia coefficient in both dilatant and pseudo-plastic fluids.

Problem formulation

Steady, incompressible and laminar fully developed flow of the power law fluid with constant properties in a long duct of rectangular cross section, as shown in Figure 1, is carried out. Fully developed energy equation is solved subject to constant heat flux with peripheral constant wall temperature, known as $H1$ thermal boundary condition [19]. Under the above assumptions, z -component of momentum equation will get the form by applying the Darcy–Brinkman–Forchheimer model as has been taken in [17] for their case study:

$$\frac{\partial}{\partial x} \left\{ \mu \frac{\partial w}{\partial x} \right\} + \frac{\partial}{\partial y} \left\{ \mu \frac{\partial w}{\partial y} \right\} = \frac{dp}{dz} - \frac{m\epsilon^n}{K} w^n - \frac{F^* \epsilon^2}{K^{1/2}} w^2 \quad (1)$$

where p is the pressure, w is the velocity in the axial direction, μ , m and n are the apparent viscosity, flow consistency index and power law model of the power law fluid respectively, while ϵ , F^* and K are the porosity, empirical constant and permeability respectively. Equation (1) is solved by using the no slip boundary condition at solid boundaries:

$$w = 0 \quad \text{at} \quad x = 0 \quad \text{for} \quad 0 \leq y \leq b$$

$$w = 0 \quad \text{at} \quad y = 0 \quad \text{for} \quad 0 \leq x \leq a$$

$$w = 0 \quad \text{at} \quad x = a \quad \text{for} \quad 0 \leq y \leq b$$

$$w = 0 \quad \text{at} \quad y = b \quad \text{for} \quad 0 \leq x \leq a$$

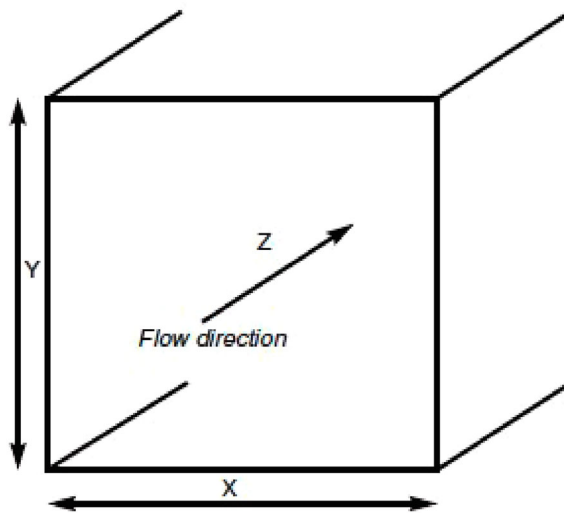


Figure 1. Cross section of an independent duct.

Apparent viscosity, μ for the power law fluid is defined as:

$$\mu = m \left\{ \left(\frac{\partial w}{\partial x} \right)^2 + \left(\frac{\partial w}{\partial y} \right)^2 \right\}^{0.5(n-1)} \quad (2)$$

In the absence of Darcy–Brinkman–Forchheimer model, the above mathematical model gets the form as has been taken in the study [15], in the absence of the magnetic field.

For maximum heat transfer rate, axial heat conduction and free convection are not taken into account; therefore, the law of conservation of energy can be expressed for this study as:

$$\frac{\partial}{\partial x} \left\{ \frac{\partial T}{\partial x} \right\} + \frac{\partial}{\partial y} \left\{ \frac{\partial T}{\partial y} \right\} = \frac{c_p \rho}{\kappa} \frac{\partial T}{\partial z} \quad (3)$$

where κ is the thermal conductivity, c_p is the specific heat, ρ is the density and T is the temperature. Following $H1$ thermal boundary conditions are used to solve Equation (3), represented as:

$$T = T_w \quad \text{at} \quad x = 0 \quad \text{for} \quad 0 \leq y \leq b$$

$$T = T_w \quad \text{at} \quad y = 0 \quad \text{for} \quad 0 \leq x \leq a$$

$$T = T_w \quad \text{at} \quad x = a \quad \text{for} \quad 0 \leq y \leq b$$

$$T = T_w \quad \text{at} \quad y = b \quad \text{for} \quad 0 \leq x \leq a$$

where T_w is the constant wall temperature.

To solve the governing system of partial differential equations, we transform in dimensionless form using the following parameters:

$$X = \frac{x}{a}, \quad Y = \frac{y}{a}, \quad \beta = \frac{b}{a} \quad (4)$$

$$W = \frac{w}{w_r}, \quad w_r = \left\{ \left(-\frac{dP}{dz} \right) \frac{a^{(n+1)}}{m} \right\}^{1/n} \quad (5)$$

$$\hat{\mu} = \frac{\mu}{\mu_r}, \quad \mu_r = m^{1/n} \left\{ a \left(-\frac{dP}{dz} \right) \right\}^{(n-1)/n} \quad (6)$$

$$\tau = \kappa \frac{T - T_w}{\dot{Q}'} \quad (7)$$

where β is the aspect ratio, w_r is the reference velocity, μ_r is the reference viscosity and \dot{Q}' is the heat transfer rate per unit axial length.

With the help of Equations (4)–(6), Equations (1) and (2) will reduce in the following form with boundary conditions:

$$\frac{\partial}{\partial X} \left\{ \hat{\mu} \frac{\partial W}{\partial X} \right\} + \frac{\partial}{\partial Y} \left\{ \hat{\mu} \frac{\partial W}{\partial Y} \right\} = -1 + \frac{W^n}{Da} + \frac{Fr}{Da} W^2 \quad (8)$$

$$\hat{\mu} = \left\{ \left(\frac{\partial W}{\partial X} \right)^2 + \left(\frac{\partial W}{\partial Y} \right)^2 \right\}^{0.5(n-1)} \quad (9)$$

$$W = 0 \quad \text{at} \quad X = 0 \quad \text{for} \quad 0 \leq y \leq \beta$$

$$W = 0 \quad \text{at} \quad Y = 0 \quad \text{for} \quad 0 \leq x \leq 1$$

$$W = 0 \quad \text{at} \quad X = 1 \quad \text{for} \quad 0 \leq Y \leq \beta$$

$$W = 0 \quad \text{at} \quad Y = \beta \quad \text{for} \quad 0 \leq X \leq 1$$

where Da is the Darcy parameter and Fr is the inertia coefficient. For the sake of completeness, we use the following relations as have been used by [20] in Equation (3):

$$\frac{\partial T}{\partial z} = \frac{dT_w}{dz} = \frac{dT_b}{dz} = \frac{\dot{Q}'}{\rho c_p A_c w_m} \quad (10)$$

where w_m is the mean velocity and A_c is the cross sectional area of the rectangular duct. Energy Equation (3) will take the form by using the Equation (10):

$$\frac{\partial}{\partial X} \left\{ \frac{\partial T}{\partial X} \right\} + \frac{\partial}{\partial Y} \left\{ \frac{\partial T}{\partial Y} \right\} = \frac{\dot{Q}'}{\kappa} \frac{w}{w_m A_c} \quad (11)$$

By using Equations (4)–(7), we get:

$$\frac{\partial}{\partial X} \left\{ \frac{\partial \tau}{\partial X} \right\} + \frac{\partial}{\partial Y} \left\{ \frac{\partial \tau}{\partial Y} \right\} = \frac{W}{W_m \hat{A}_c} \quad (12)$$

Corresponding thermal boundary conditions are:

$$\tau = 0 \quad \text{at} \quad X = 0 \quad \text{for} \quad 0 \leq y \leq \beta$$

$$\tau = 0 \quad \text{at} \quad Y = 0 \quad \text{for} \quad 0 \leq x \leq 1$$

$$\tau = 0 \quad \text{at} \quad X = 1 \quad \text{for} \quad 0 \leq Y \leq \beta$$

$$\tau = 0 \quad \text{at} \quad Y = \beta \quad \text{for} \quad 0 \leq X \leq 1$$

Geometrical symmetry allows us to take only quarter of the duct as a computational domain due to the same flow behavior along X - and Y -axis. Therefore, our domain will become:

$$0 \leq X \leq 0.5 \quad (13)$$

$$0 \leq Y \leq 0.5\beta \quad (14)$$

Now we transform the governing system of equations into discretized form by integrating over the differential volume, $dV = dXdY$ of the typical control volume, as shown in Figure 2. By applying the above procedure, we get:

$$A_E W_E + A_N W_N - A_P W_P + A_W W_W + A_S W_S = S_W \quad (15)$$

where A_E and A_W are neighboring east and west velocity nodes coefficient, while A_N and A_S are neighboring north and south velocity nodes coefficient of central velocity node, W_P , and S_W is the velocity source term. A_E , A_W , A_N and A_S are determined as:

$$A_E = \frac{a_e \hat{\mu}_e}{dX} \quad (16)$$

$$A_W = \frac{a_w \hat{\mu}_w}{dX} \quad (17)$$

$$A_N = \frac{a_n \hat{\mu}_n}{dY} \quad (18)$$

$$A_S = \frac{a_s \hat{\mu}_s}{dY} \quad (19)$$

where e , w , n and s are the faces of the control volume, while a_e , a_s , a_n and a_s are the face areas of control volume. A_P and S_W are determined as:

$$A_P = A_E + A_N + A_W + A_S + \frac{W_P^{(n-1)}}{Da} dXdY + \frac{Fr W_P}{Da} dXdY \quad (20)$$

$$S_W = -dXdY \quad (21)$$

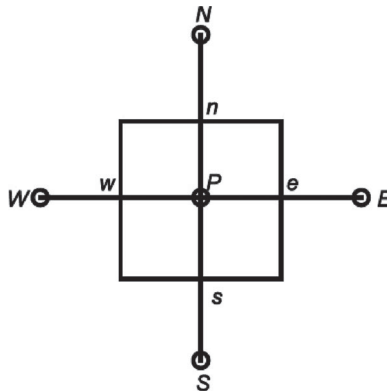


Figure 2. Typical control volume.

Apparent viscosity, $\hat{\mu}$, is calculated at the central face of control volume as:

$$\hat{\mu}_P = \left[\left\{ \frac{W_e - W_w}{dX} \right\}^2 + \left\{ \frac{W_n - W_s}{dY} \right\}^2 \right]^{0.5(n-1)} \quad (22)$$

Equation (12) will become in discretized form:

$$B_E \tau_E + B_N \tau_N - B_P \tau_P + B_W \tau_W + B_S \tau_S = S_\tau \quad (23)$$

where B_E and B_W are neighboring east and west temperature node coefficient, while B_N and B_S are neighboring north and south temperature node coefficient of the central temperature node, τ_P , and S_τ is the temperature source term. B_E , B_W , B_N and B_S are determined as:

$$B_E = \frac{a_e}{dX} \quad (24)$$

$$B_W = \frac{a_w}{dX} \quad (25)$$

$$B_N = \frac{a_n}{dY} \quad (26)$$

$$B_S = \frac{a_s}{dY} \quad (27)$$

B_P and S_τ are determined as:

$$B_P = B_E + B_N + B_W + B_S \quad (28)$$

$$S_\tau = \frac{W_P}{W_m \hat{A}_c} dX dY \quad (29)$$

To solve the coupled discretized Equations (15) and (23), we use the well-known technique strongly implicit procedure (SIP) [21] because of its fast convergence. With the help of velocity and temperature, the fanning friction factor, fRe and average Nusselt number, Nu , are determined to discuss the flow and heat transfer rate of power law fluid for different values of power law model, n . Fanning friction factor, fRe , is defined by relation as:

$$fRe = \frac{D_h^{(n+1)}}{2W_m^n} \quad (30)$$

where D_h is the hydraulic diameter (i.e. length). Average Nusselt number, Nu , is defined as:

$$Nu = - \frac{D_h}{H_P \tau_b} \quad (31)$$

where H_P and τ_b are the heated perimeter and bulk mean temperature.

Validation with literature

To validate the results with literature, we plot the velocity profiles in the absence of Darcy–Brinkman–Forchheimer model, as presented in the Figure 3. By comparing velocity profiles with Figure 4a, 4b and 4c of [15] in the absence of Lorentz force at $n = 1.5$, $n = 1.0$ and $n = 0.5$, we can see that velocity profiles match with each other.

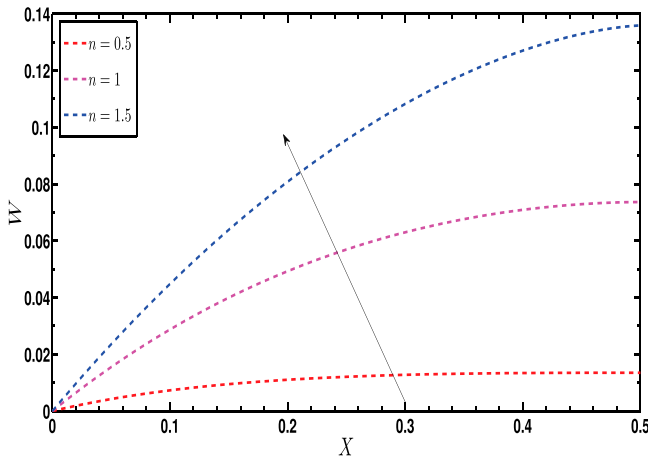


Figure 3. Limiting case W vs X at $\beta = 1$.

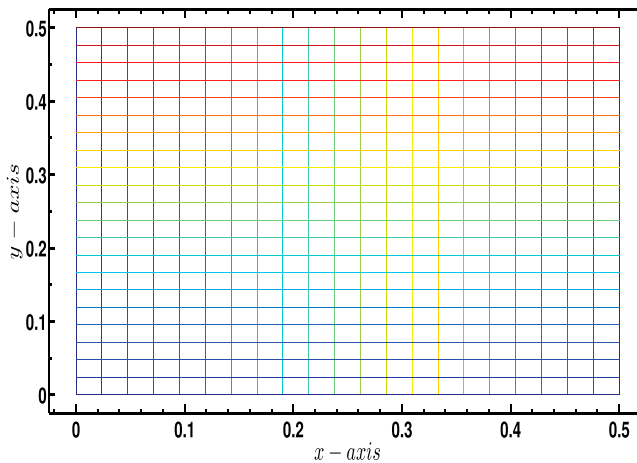


Figure 4. Coarsest grid size ($21 \times 21 = 441$).

Grid-independent analysis

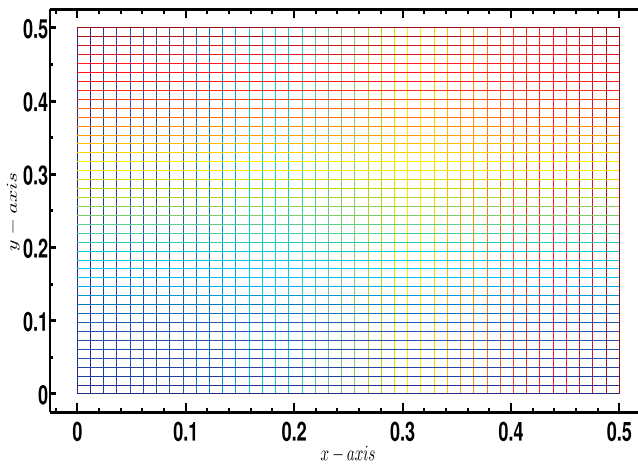
Grid-independent analysis is taken into account to select the number of control volumes, (CVs), having the same dimension along x -axis and y -axis, in the computational domain. For this purpose, we compute % difference of fRe and Nu by comparing the calculated results at previous step, as presented in Table 1. Four grid size i.e. coarsest, coarse, fine and finest are shown in Figures 4–7. We can be seen that % difference is overall less than 1% in all grid sizes. However, the decrease in % difference reduces, when we take the CVs of fine grid size and further. Therefore, we select $81 \times 81 = 6561$ number of CVs to carry out the further study.

Results and discussion

Now for the further study, we adopt the following range of parameters:

Table 1. Grid-independent analysis for different number of control volumes, (CVs), at $Fr = 10$, $Da = 0.1$, $n = 1.5$ and $\beta = 1$.

CVs	fRe	% difference	Nu	% difference
121	64.87599	–	3.75812	–
441	65.05348	0.2728	3.74490	0.3530
961	64.90042	0.2358	3.74831	0.0910
1681	64.77022	0.2007	3.75194	0.0967
2601	64.67220	0.1519	3.75483	0.0770
3721	64.59756	0.1156	3.75707	0.0596
5041	64.53883	0.0910	3.75884	0.0471
6561	64.49190	0.0728	3.76026	0.0378
8281	64.45303	0.0603	3.76143	0.0311
10201	64.42032	0.0508	3.76241	0.0260

**Figure 5.** Coarse grid size ($(41 \times 41 = 1681)$).

Power law model:

$$n = 0.5, 0.7, 0.9, 1, 1.1, 1.3, 1.5 \quad (32)$$

Darcy parameter:

$$Da = 0.01, 100 \quad (33)$$

Inertia coefficient:

$$Fr = 0.01, 0.1, 1, 10, 100 \quad (34)$$

Aspect ratio:

$$\beta = 1, 0.5, 0.2 \quad (35)$$

Now we discuss the flow behavior of power law fluid against different parameters. Figures 8–11 are used to study the flow behavior of the power law fluids for different values of Da and Fr at $\beta = 1$. From each figure, we can observe the opposite trend, when we increase the value of n in the case of dilatant fluids and, decrease the value of n in the case of pseudo-plastic fluids. This means that the velocity has a direct relationship with n and inverse relationship with n in the case of dilatant and pseudo-plastic fluids respectively, as has been observed by [8] in literature. By increasing/decreasing the value of n

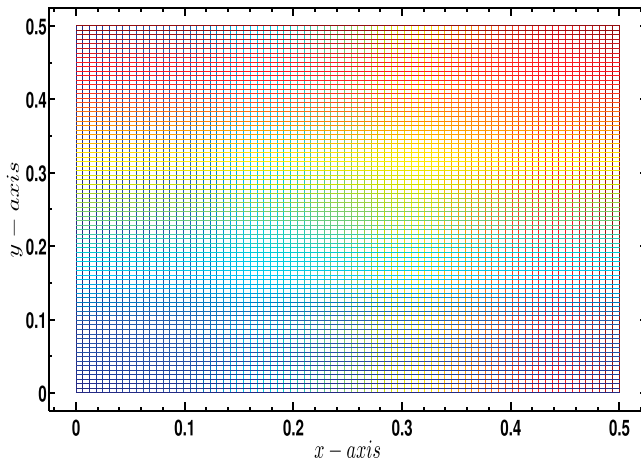


Figure 6. Fine grid size ($81 \times 81 = 6561$).

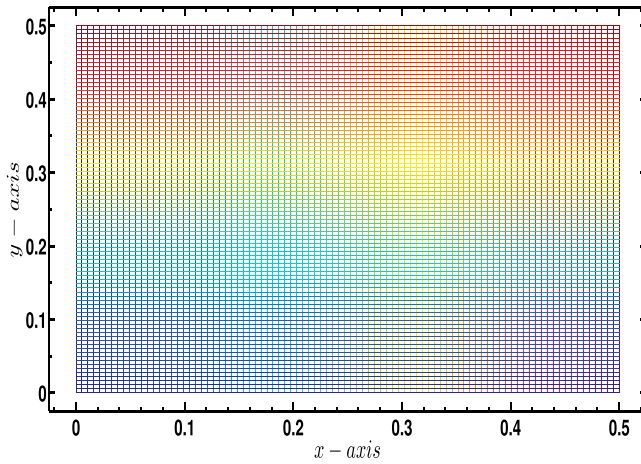


Figure 7. Finest grid size ($91 \times 91 = 8281$).

in dilatant/pseudo-plastic fluids, the shear rate increases / decreases. This elucidates as increase/decrease in the velocity.

By comparing Figures 8 and 9 with Figures 10 and 11, we can observe the effect of inertia coefficient apparently on the velocity profiles in the case of dilatant and Newtonian fluids, while inertia coefficient effect dominates in the case of Pseudo-plastic fluids. Fact is that the inertia force depends upon the dense growth of fluid. By increasing the value of n in dilatant fluid, the effect of inertia coefficient becomes more apparent due to increase in the shear rate. The velocity profiles behave alike in the case of dilatant fluid, ($n = 1.5$), Newtonian fluid ($n = 1$) and Pseudo-plastic fluid ($n = 0.5$) at $Da = 100$, when we compare velocity profile of [15] in the absence of a magnetic field. Therefore, it can be concluded that Forchheimer term can not be excluded from the Navier Stokes equation especially in the case of dilatant fluid, when Darcy parameter is kept to be less than one (i.e. $Da < 1$).

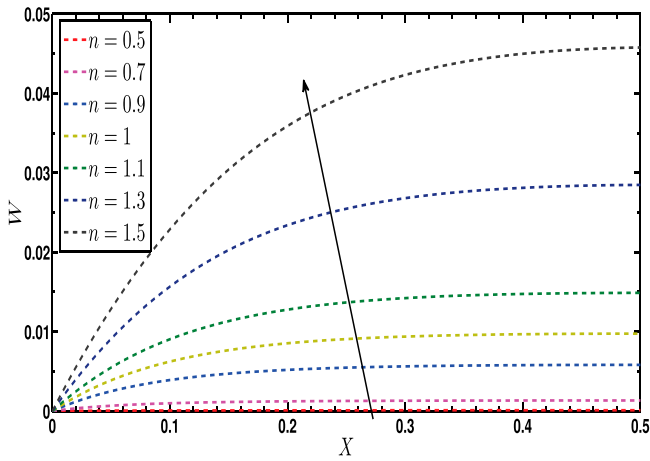


Figure 8. W vs X for different values of n at $Da = 0.01$, $Fr = 0.01$ and $\beta = 1$.

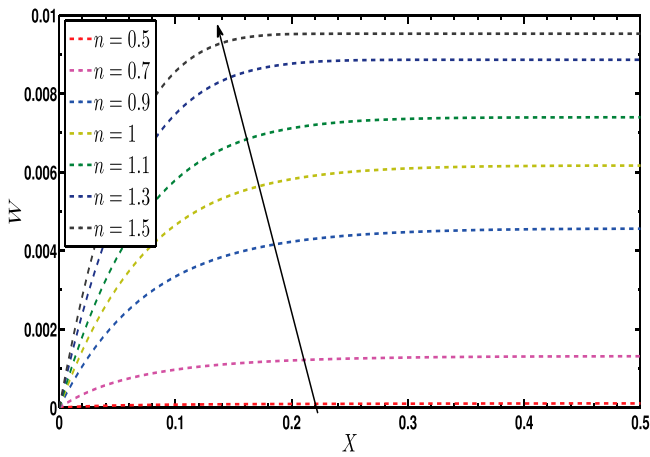


Figure 9. W vs X for different values of n at $Da = 0.01$, $Fr = 100$ and $\beta = 1$.

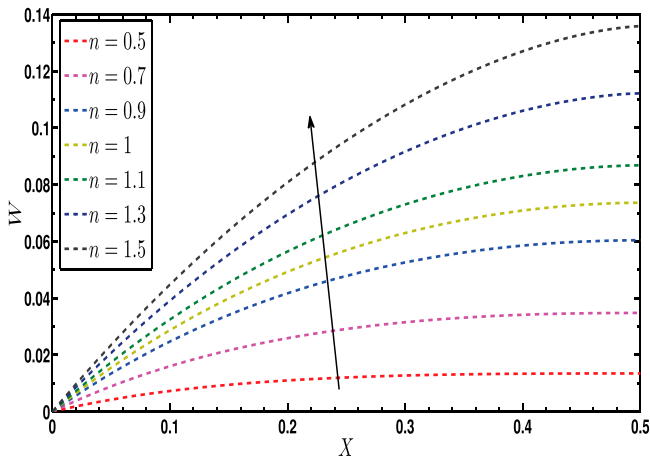


Figure 10. W vs X for different values of n at $Da = 100$, $Fr = 0.01$ and $\beta = 1$.

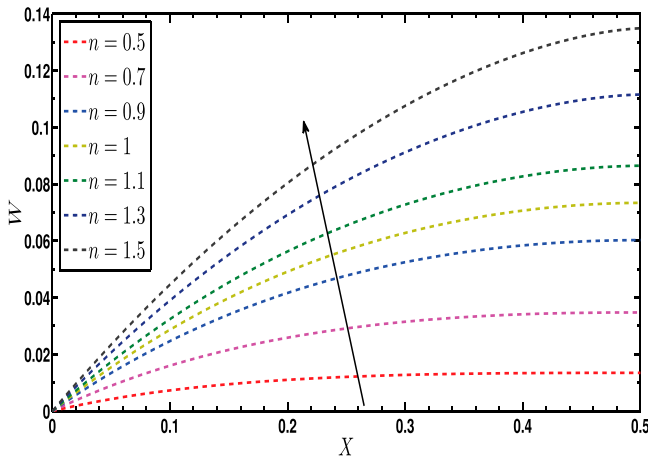


Figure 11. W vs X for different values of n at $Da = 100$, $Fr = 100$ and $\beta = 1$.

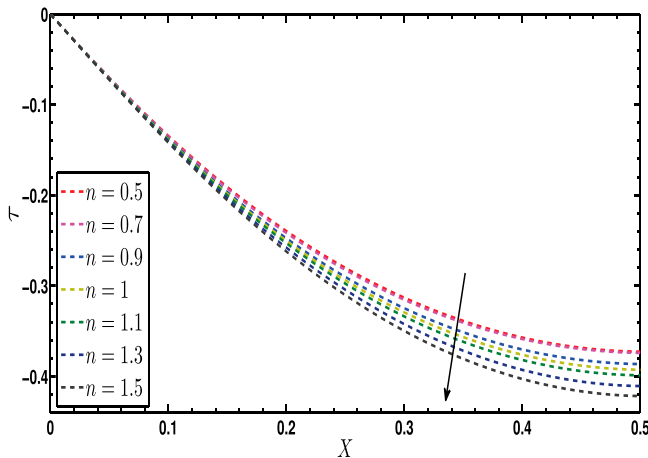


Figure 12. τ vs X for different values of n at $Da = 0.01$, $Fr = 0.01$ and $\beta = 1$.

Figures 12–15 are used to study the forced convection behavior of the power law fluid for different values of Da and Fr at $\beta = 1$. From each figure, we can note the opposite relationship of n with the temperature in the case of dilatant and pseudo-plastic fluids as have been discussed in Figures 8–11 except Figure 13. The impact of n on the temperature profiles has been changed from inverse to direct relationship, when we increase the inertia coefficient term from 0.01 to 100. It is because of the strength of the inertial force as explained in Figures 8 and 9. By comparing Figures 10 and 11 with Figures 14 and 15, no deviation has been observed in the temperature profiles, when we increase the value of Fr .

Now we tabulate the numerical results. Tables 2–5 show the variation of fRe and Nu by changing the value of aspect ratio, Darcy Parameter, inertia coefficient and power law model. Same thing has been noted here from Tables 2 and 5 as discussed in Figures 8–15, when we see the variation of fRe and Nu against n , Da and Fr . From Tables 2–4, we can observe the inverse variation in fRe by decreasing the value of aspect ratio. When we

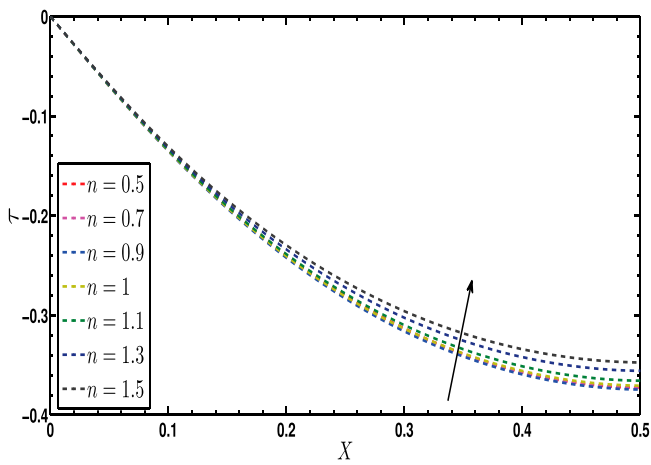


Figure 13. τ vs X for different values of n at $Da = 0.01, Fr = 100$ and $\beta = 1$.

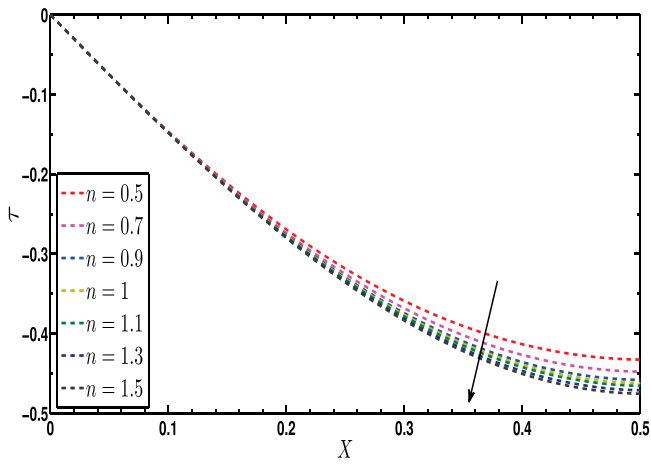


Figure 14. τ vs X for different values of n at $Da = 100, Fr = 0.01$ and $\beta = 1$.

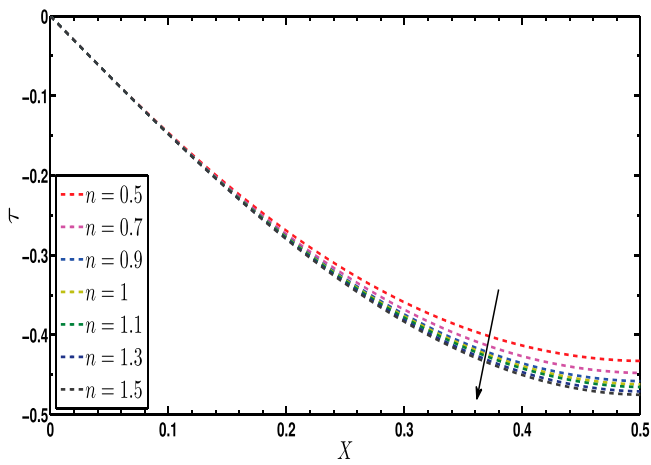


Figure 15. τ vs X for different values of n at $Da = 100, Fr = 100$ and $\beta = 1$.

Table 2. Effects of n , Da and Fr on W_m , fRe , τ_b and Nu at $\beta = 1$.

n	Da	Fr	W_m	fRe	τ_b	Nu		
1.5	0.01	0.01	0.026611042	115.180029	-0.2468241	4.051467		
		0.1	0.026416545	116.454421	-0.2463228	4.059714		
		1	0.024735995	128.521542	-0.2419156	4.133673		
		10	0.017348017	218.824155	-0.2209785	4.525327		
	100	100	0.007866296	716.662326	-0.1890992	5.288230		
		0.01	0.058747907	35.114089	-0.2870305	3.483950		
		0.1	0.058747586	35.114377	-0.2870303	3.483953		
		1	0.058744740	35.116929	-0.2870280	3.483981		
		10	0.058716503	35.142264	-0.2870050	3.484260		
		100	0.058436510	35.395137	-0.2867766	3.487034		
		0.5	0.01	0.01	0.000077289	56.873554	-0.2024916	4.938478
				0.1	0.000077317	56.863484	-0.2025293	4.937556
1	0.000077290			56.873242	-0.2024909	4.938493		
10	0.000077322			56.861663	-0.2025309	4.937518		
100	100		0.000077289	56.873800	-0.2024858	4.938617		
	0.01		0.007788106	5.665706	-0.2545435	3.928601		
	0.1		0.007788103	5.665708	-0.2545435	3.928601		
	1		0.007788072	5.665718	-0.2545434	3.928603		
	10		0.007787921	5.665774	-0.2545430	3.928610		
	100		0.007786394	5.666329	-0.2545382	3.928682		

Table 3. Effects of n , Da and Fr on W_m , fRe , τ_b and Nu at $\beta = 0.5$.

n	Da	Fr	W_m	fRe	τ_b	Nu		
1.5	0.01	0.01	0.003431463	902.657257	-0.2154564	4.125610		
		0.1	0.003431258	902.738203	-0.2154504	4.125724		
		1	0.003429211	903.546461	-0.2153904	4.126872		
		10	0.003408864	911.648237	-0.2147955	4.138304		
	100	100	0.003219556	993.225482	-0.2091974	4.249043		
		0.01	0.003467532	888.609800	-0.2163090	4.109348		
		0.1	0.003467532	888.609808	-0.2163090	4.109348		
		1	0.003467532	888.609889	-0.2163090	4.109348		
		10	0.003467530	888.610693	-0.2163089	4.109349		
		100	0.003467509	888.618736	-0.2163083	4.109361		
		0.5	0.01	0.01	0.000000942	280.328428	-0.1880022	4.728077
				0.1	0.000000942	280.328737	-0.1880003	4.728125
1	0.000000942			280.346855	-0.1879853	4.728502		
10	0.000000941			280.510915	-0.1878460	4.732010		
100	100		0.000000949	279.347406	-0.1887345	4.709733		
	0.01		0.000001097	259.883710	-0.1910200	4.653382		
	0.1		0.000001097	259.883710	-0.1910200	4.653382		
	1		0.000001097	259.883712	-0.1910200	4.653382		
	10		0.000001097	259.883729	-0.1910200	4.653382		
	100		0.000001097	259.883900	-0.1910198	4.653385		

decrease the value of aspect ratio, the cross section of the duct decreases. This elucidates as restricted in the fluid flow and therefore, causes increase in fRe . Mixed variations have been observed in the case of Nu . Nu increases when we decrease the aspect ratio from 1 to 0.5, whereas Nu increases by further decreasing from 0.5 to 0.2. Furthermore, by decreasing the value of aspect ratio, the effects of Darcy Parameter and inertia coefficient become down due to decrease in flow domain.

Table 4. Effects of n , Da and Fr on W_m , fRe , τ_b and Nu at $\beta = 0.2$.

n	Da	Fr	W_m	fRe	τ_b	Nu	
1.5	0.01	0.01	0.000799617	1418.54770	-0.1072609	5.179477	
		0.1	0.000799614	1418.55443	-0.1072607	5.179486	
		1	0.000799589	1418.62180	-0.1072588	5.179580	
		10	0.000799336	1419.29551	-0.1072394	5.180519	
	100	100	0.000796815	1426.03543	-0.1070459	5.189881	
		0.01	0.000800532	1416.11657	-0.1073176	5.176744	
		0.1	0.000800532	1416.11657	-0.1073176	5.176744	
		1	0.000800532	1416.11657	-0.1073176	5.176744	
	0.5	0.01	10	0.000800532	1416.11664	-0.1073176	5.176744
			100	0.000800531	1416.11732	-0.1073175	5.176745
			0.01	0.000000041	476.585838	-0.1618963	3.431551
			0.1	0.000000041	476.590289	-0.1619000	3.431473
100		1	0.000000041	476.635372	-0.1618929	3.431625	
		10	0.000000041	476.961412	-0.1618646	3.432225	
		100	0.000000040	479.383325	-0.1612981	3.444279	
		0.01	0.000001097	259.883710	-0.1910200	4.653382	
		0.1	0.000001097	259.883710	-0.1910200	4.653382	
		1	0.000001097	259.883712	-0.1910200	4.653382	
		10	0.000001097	259.883729	-0.1910200	4.653382	
		100	0.000001097	259.883901	-0.1910198	4.653386	

Table 5. Effects of Fr , Da and n on W_m , fRe , τ_b and Nu at $\beta = 1$.

Da	Fr	n	W_m	fRe	τ_b	Nu		
0.01	10	0.5	0.000077322	56.861663	-0.2025309	4.937518		
		0.7	0.000970332	64.287385	-0.2064826	4.843024		
		0.9	0.003903141	73.569395	-0.2161583	4.626239		
		1	0.006149408	81.308639	-0.2197041	4.551576		
		1.1	0.008661808	92.811243	-0.2219469	4.505582		
		1.3	0.013521494	134.473877	-0.2229218	4.485877		
		1.5	0.017348017	218.824155	-0.2209785	4.525327		
		100	0.5	0.000077289	56.873800	-0.2024858	4.938617	
			0.7	0.000955139	65.001493	-0.2057533	4.860189	
			0.9	0.003321944	85.058340	-0.2084885	4.796428	
			1	0.004591342	108.900632	-0.2061769	4.850204	
			1.1	0.005650172	148.491708	-0.2028061	4.930817	
			1.3	0.007077879	311.957879	-0.1956357	5.111542	
		100	10	1.5	0.007866296	716.662326	-0.1890992	5.288230
				0.5	0.007787921	5.665774	0.2545430	3.928610
0.7	0.018300230			8.227169	-0.2661837	3.756804		
0.9	0.029645404			11.863378	-0.2740708	3.648692		
1	0.035136239			14.230322	-0.2770977	3.608835		
1.1	0.040417799			17.050616	-0.2796966	3.575303		
1.3	0.050115875			24.490750	-0.2838424	3.523082		
1.5	0.058716503			35.142263	-0.2870050	3.484260		
100	0.5			0.007786394	5.666329	-0.2545383	3.928682	
	0.7			0.018284644	8.232078	-0.26615730	3.757177	
	0.9			0.029590812	11.883074	-0.2740037	3.649586	
	1			0.035052722	14.264228	-0.2770055	3.610037	
	1.1			0.040300040	17.105429	-0.2795774	3.576828	
	1.3			0.049919926	24.615796	-0.2836677	3.525251	
1.5	0.058436510			35.395137	-0.2867766	3.487034		

Conclusion

Here we have taken the Darcy–Brinkman–Forchheimer model to describe the fully developed flow behavior of power law fluid through rectangular duct. Energy equation is solved subject to constant heat flux with the peripheral constant wall temperature, known as

$H1$ thermal condition. It has been concluded that the inertia coefficient effect can not be neglected at $Da = 0.01$ and $\beta = 1$ due to direct variation of fRe and Nu in the case of dilatant fluid. Furthermore, the inertia coefficient effect becomes down in both cases of $Da = 0.01$ and 100 in pseudo-plastic fluid and, by decreasing the value of the aspect ratio.

Disclosure statement

No potential conflict of interest was reported by the author(s).

References

- [1] Nield DA, Bejan A Convection in porous media. 3rd ed. New York (NY): Springer; 2006.
- [2] Hooman K, Haji-Sheikh A, Nield DA. Thermally developing Brinkman–Brinkman forced convection in rectangular ducts with isothermal walls. *Int J Heat Mass Transf.* 2007;50:3521–3533.
- [3] Chen GM, Tso CP. A two-equation model for thermally developing forced convection in porous medium with viscous dissipation. *Int J Heat Mass Transf.* 2011;54:5406–5414.
- [4] Ouyang XL, Vafai K, Jiang PX. Analysis of thermally developing flow in porous media under local thermal non-equilibrium conditions. *Int J Heat Mass Transf.* 2013;67:768–775.
- [5] Kolutawong C, Kananai N, Giacomini AJ, et al. Viscous dissipation of a power law fluid in axial flow between isothermal eccentric cylinders. *J Nonnewton Fluid Mech.* 2011;166(1–2):133–144.
- [6] Park S, Irvine TF, Capobianchi M. Experimental and numerical study of friction factor for a modified power law fluid in a rectangular duct. *Exp Therm Fluid Sci.* 1994;9(1):61–68.
- [7] Griffiths PT, Garrett SJ, Stephen SO. The neutral curve for stationary disturbances in rotating disk flow for power-law fluids. *J Nonnewton Fluid Mech.* 2014;213:73–81.
- [8] Ahmed F, Iqbal M, Akbar NS. Numerical study of forced convective power law fluid flow through an annulus sector duct. *Eur Phys J Plus.* 2016;131(9):341–359.
- [9] Khan M, Khan WA. MHD boundary layer flow of a power law nanofluid with new mass flux condition. *AIP Adv.* 2016;6:1–9.
- [10] Ahmed F, Iqbal M. MHD power law fluid flow and heat transfer analysis through Darcy Brinkman porous media in annular sector. *Int J Mech Sci.* 2017;130:508–517.
- [11] Ahmed F, Iqbal M, Pop I. Numerical simulation of forced convective power law nanofluid through circular annulus sector. *J Therm Anal Calorim.* 2019;135(2):861–871.
- [12] Ahmed F, Iqbal M. Heat transfer analysis of MHD power law nano fluid flow through annular sector duct. *J Therm Sci.* 2020;29(1):169–181.
- [13] Kumar A, Dhiman A, Baranyi L. CFD analysis of power-law fluid flow and heat transfer around a confined semi-circular cylinder. *Int J Heat Mass Transf.* 2015;82:159–169.
- [14] Lin Y, Zheng L, Li B, et al. A new diffusion for laminar boundary layer flow of power law fluids past a flat surface with magnetic effect and suction or injection. *Int J Heat Mass Transf.* 2015;90:1090–1097.
- [15] Ahmed MES. Numerical solution of power law fluids flow and heat transfer with a magnetic field in a rectangular duct. *Int Commun Heat Mass Transf.* 2006;33(9):1165–1176.
- [16] Chen GM, Tso CP. Effects of viscous dissipation on forced convective heat transfer in a channel embedded in a power-law fluid saturated porous medium. *Int Commun Heat Mass Transf.* 2011;38:57–62.
- [17] Elgazery NS. An implicit-Chebyshev pseudospectral method for the effect of radiation on power-law fluid past a vertical plate immersed in a porous medium. *Commun Nonlinear Sci Numer Simul.* 2018;13:728–744.
- [18] Avramenko AA, Shevchuk IV, Kovetskaya MM, et al. Darcy-Brinkman-Forchheimer model for film boiling in porous media. *Transp Porous Media.* 2020;134:503–536.
- [19] Shah RK, London AL. Laminar flow forced convection in ducts. London: Academic Press; 1978.
- [20] Iqbal M, Afaq H. Fluid flow and heat transfer through an annular sector duct filled with porous media. *J Porous Media.* 2015;18(7):679–687.
- [21] Peric M, Ferziger JH. Computational methods for fluid dynamics. Berlin (Germany): Springer; 2002.